Acta Crystallographica Section D
Biological Crystallography
ISSN 0907-4449

Staphylococcus aureus thiaminase II: oligomerization warrants proteolytic protection against serine proteases

Afshan Begum,[a]‡ Julia Drebes,[a,b]‡ Alexey Kikhney,[c] Ingrid B. Müller,[b] Markus Perbandt,[a,d] Dmitri Svergun,[c] Carsten Wrenger[e]* and Christian Betzel[a]*

[a]Laboratory for Structural Biology of Infection and Inflammation, University of Hamburg, c/o DESY, Notkestrasse 85, Building 22A, 22603 Hamburg, Germany, [b]Department of Biochemistry, Bernhard Nocht Institute for Tropical Medicine, Bernhard Nocht Strasse 74, 20359 Hamburg, Germany, [c]EMBL Hamburg, c/o DESY, Notkestrasse 85, Building 25A, 22603 Hamburg, Germany, [d]Department of Medical Microbiology, Virology and Hygiene, University Medical Center Hamburg-Eppendorf, Martinistrasse 52, 20246 Hamburg, Germany, and [e]Unit for Drug Discovery, Department of Parasitology, Institute of Biomedical Science, University of São Paulo, Avenida Professor Lineu Prestes 1374, 05508-000 São Paulo-SP, Brazil

‡ These authors contributed equally to this work.

Correspondence e-mail: cwrenger@icb.usp.br, christian.betzel@uni-hamburg.de

Received 12 April 2013
Accepted 1 August 2013

PDB Reference: thiaminase II, 4fn6

Staphylococcus aureus TenA (*Sa*TenA) is a thiaminase type II enzyme that catalyzes the deamination of aminopyrimidine, as well as the cleavage of thiamine into 4-amino-5-hydroxymethyl-2-methylpyrimidine (HMP) and 5-(2-hydroxyethyl)-4-methylthiazole (THZ), within thiamine (vitamin B_1) metabolism. Further, by analogy with studies of *Bacillus subtilis* TenA, *Sa*TenA may act as a regulator controlling the secretion of extracellular proteases such as the subtilisin type of enzymes in bacteria. Thiamine biosynthesis has been identified as a potential drug target of the multi-resistant pathogen *S. aureus* and therefore all enzymes involved in the *S. aureus* thiamine pathway are presently being investigated in detail. Here, the structure of *Sa*TenA, determined by molecular replacement and refined at 2.7 Å resolution to an *R* factor of 21.6% with one homotetramer in the asymmetric unit in the orthorhombic space group $P2_12_12_1$, is presented. The tetrameric state of wild-type (WT) *Sa*TenA was postulated to be the functional biological unit and was confirmed by small-angle X-ray scattering (SAXS) experiments in solution. To obtain insights into structural and functional features of the oligomeric *Sa*TenA, comparative kinetic investigations as well as experiments analyzing the structural stability of the WT *Sa*TenA tetramer *versus* a monomeric *Sa*TenA mutant were performed.

1. Introduction

Infections with methicillin-resistant *Staphylococcus aureus* (MRSA) are known to have serious health implications, including complicated skin infections, pneumonia or meningitis and osteomyelitis (Fey *et al.*, 2003; Lowy, 1998). Owing to the development of distinct abilities, such as the invasion of host cells, the pathogen escapes the human immune system (Lowy, 1998; Powers & Bingham, 1990; Kauffman *et al.*, 1993). Additionally, the bacterium has developed resistance against various antibiotics, which causes difficulties in therapeutic interventions, especially in immune-deficient patients (Tumbarello *et al.*, 1998; Weinke *et al.*, 1992). The disastrous emergence of drug resistance demands urgent and continuous research to discover and subsequently develop novel chemotherapeutics (Spellberg *et al.*, 2013). Ideally, new drugs are generated to specifically target the pathogen, with only minimal or no toxicity to the human host (Lewis, 2012). Therefore, these drug targets need to be distinctly different from the host's metabolic processes or even to be absent in the host.

In contrast to most protozoa, plants and bacteria, mammals are unable to synthesize vitamin B_1 (thiamine) *de novo* and

thereby depend upon uptake *via* their diet. Vitamin B_1 biosynthesis in bacteria has thus been proposed to be an ideal target for drug-discovery investigations (Du *et al.*, 2011). The active form of vitamin B_1, thiamine pyrophosphate (TPP), is an essential cofactor for a variety of key enzymes in carbohydrate metabolism and amino-acid biosynthesis (Pohl *et al.*, 2004). The thiamine metabolism of *S. aureus*, consisting of six enzymes, has already been characterized (Müller *et al.*, 2009; Fig. 1). Within thiamine metabolism, TenA has two essential functions: (i) the deamination of aminopyrimidine to 4-amino-5-hydroxymethyl-2-methylpyrimidine (HMP) and (ii) acting in the hydrolysis of thiamine (Jenkins *et al.*, 2007; Toms *et al.*, 2005).

Comparative genome analysis confirmed that the *tenA* gene is associated with thiamine biosynthetic genes in bacteria. In *S. aureus*, TenA is part of the thiamine biosynthetic operon (*tenA–thiD–thiM–thiE*), which has been suggested to be regulated by TPP (Müller *et al.*, 2009). Clustering of *tenA* with the thiamine biosynthetic genes is consistent with the finding that TenA deaminates HMP precursors much more frequently than it degrades thiamine, as the deamination reaction is 100 times faster than the hydrolysis of thiamine (Jenkins *et al.*, 2007; Toms *et al.*, 2005).

In addition to its activity in thiamine biosynthesis and salvage, TenA was also assigned to have a putative function as a transcriptional regulator controlling the secretion of extracellular proteases (Pang *et al.*, 1991). Bacteria secrete a variety of virulence factors such as haemolysins, nucleases, proteases and lipases to hydrolyze host tissues (Dinges *et al.*, 2000). Pang *et al.* (1991) reported that in *Bacillus subtilis* TenA may stimulate the production of alkaline subtilisin-type proteases at a transcriptional level, on the basis that bacteria containing a multicopy plasmid encoding TenA reveal a 55-fold increase in subtilisin-type enzyme secretion.

Here, we report the structural and kinetic analysis of the TenA enzyme from *S. aureus*, which provides new insights into the *S. aureus* thiamine metabolism and might subsequently enable rational drug discovery to target the pathogen-specific vitamin B_1 biosynthetic pathway.

2. Materials and methods

2.1. Protein expression, purification, crystallization and data collection

Cloning, overexpression, purification, crystallization and X-ray diffraction data collection of wild-type *Sa*TenA were carried out as described previously (Begum *et al.*, 2011).

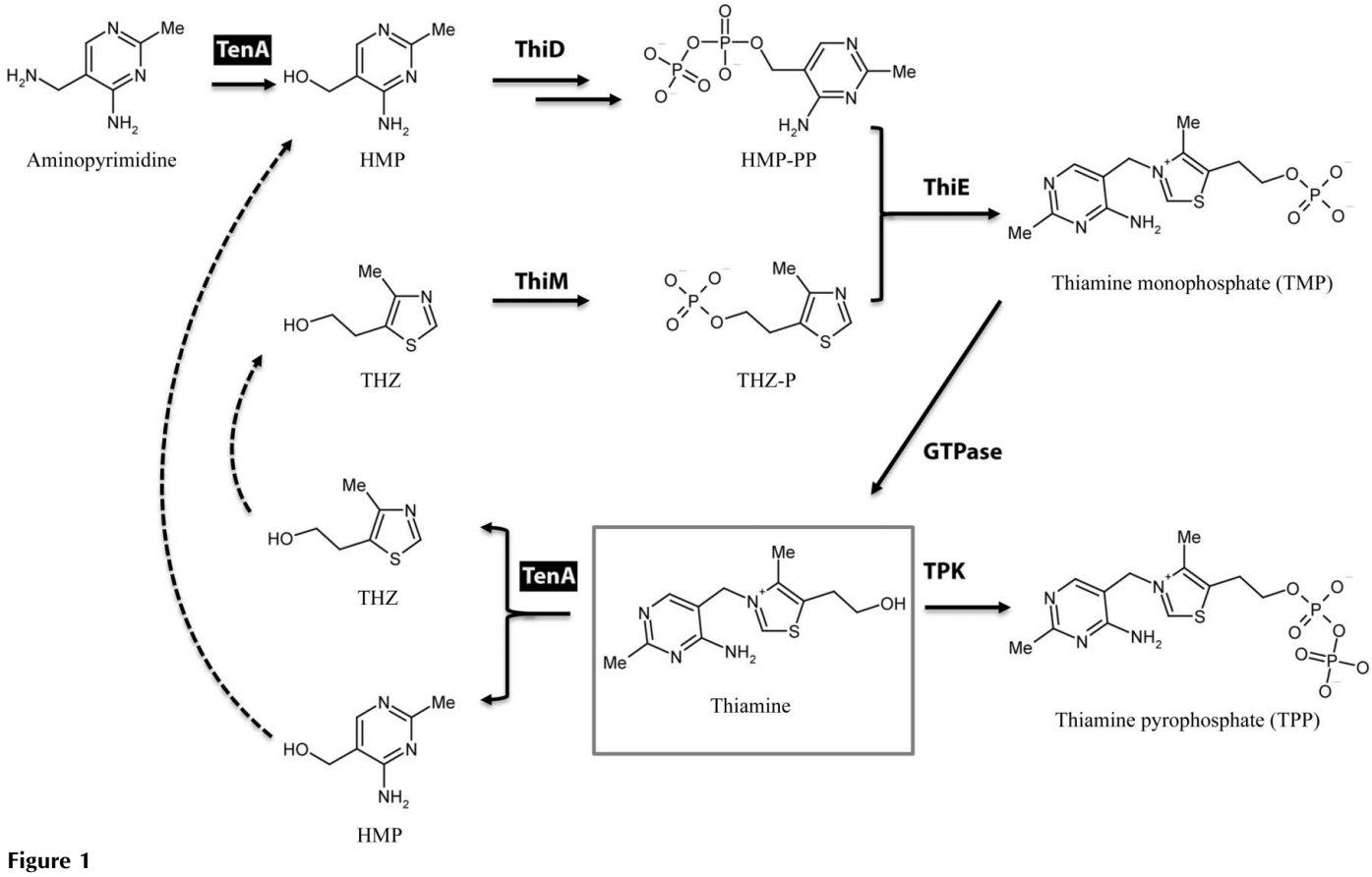

Figure 1
Scheme of the vitamin B_1 metabolism in *S. aureus* modified after Müller *et al.* (2009). Besides its function as a transcriptional regulator for subtilisin secretion, *Sa*TenA is essential in thiamine metabolism, where it is regulated by thiamine pyrophosphate (TPP) levels. It can either degrade thiamine into HMP and THZ or can deaminate aminopyrimidine to supply the biosynthetic pathway with HMP.

Table 1
Data-collection and refinement parameters.

Values in parentheses are for the highest resolution shell.

Data statistics	
Space group	$P2_12_12_1$
Unit-cell parameters (Å)	a = 103.5, b = 104.1, c = 109.6
Resolution limits (Å)	30–2.7
Total No. of reflections	424031
No. of unique reflections	31741
Multiplicity	5.1 (4.9)
Completeness (%)	95.3 (95.0)
$R_{\rm merge}$†	0.042 (0.48)
Mean $I/\sigma(I)$	23.0 (3.3)
Protomers per asymmetric unit	4
$V_{\rm M}$‡ (Å^3 Da^{-1})	2.85
Solvent content (%)	56
Refinement and model-building statistics	
Resolution range (Å)	30–2.7 (2.75–2.70)
R factor (%)	21.6
$R_{\rm free}$ (%)	25.8
No. of protein atoms	7598
No. of water atoms	81
No. of small molecules	13
R.m.s. deviations from ideal geometry	
Bond distances (Å)	0.01
Bond angles (°)	1.2
Ramachandran plot, residues in (%)	
Most favoured regions	97.6
Additional allowed regions	2.4
Disallowed regions	0.0
Average B factor (Å^2)	58.5

† $R_{\rm merge} = \sum_{hkl}\sum_i |I_i(hkl) - \langle I(hkl)\rangle| / \sum_{hkl}\sum_i I_i(hkl)$, where $\langle I(hkl)\rangle$ is the mean intensity of the observations $I_i(hkl)$ of reflection hkl. ‡ For four protomers in the asymmetric unit.

2.2. Small-angle X-ray scattering measurements

Synchrotron-radiation X-ray scattering data from solutions of *Sa*TenA were collected on the X33 beamline of the EMBL at the DORIS III storage ring (DESY, Hamburg, Germany; Blanchet *et al.*, 2012) using a photon-counting PILATUS 1M detector at a sample-to-detector distance of 2.7 m and a wavelength of 1.5 Å. Four solute concentrations in the range 1.2–7.2 mg ml^{-1} were measured. To monitor the radiation damage, eight successive 15 s exposures of all protein solutions were compared and no significant changes were observed. The data were normalized to the intensity of the transmitted beam and radially averaged. The scattering of the buffer was subtracted and the difference curves were scaled considering the protein concentration used. The low-angle data were extrapolated to infinite dilution and merged with the higher concentration data to yield the final composite scattering curve. The data-processing steps were performed using the programs *DATOP* and *ALMERGE* (Franke *et al.*, 2012).

2.3. Crystal structure determination and refinement

The crystal structure was solved by molecular replacement with *MOLREP* (Vagin & Teplyakov, 2010) using the 1.65 Å resolution crystal structure of thiaminase type II from *S. epidermidis* (PDB entry 3no6; sequence identity 58%; Joint Center for Structural Genomics, unpublished work) as a search model. The initial R factor for all data between 15.0 and 3.5 Å resolution was 45.8%. For further refinement *REFMAC*5 (Murshudov *et al.*, 2011) from the *CCP*4 v.4.2 software suite (Winn *et al.*, 2011) was applied, and the graphics program *Coot* (Emsley & Cowtan, 2004) was used for model building. Subsequent refinement and model building of strands and surface loops, adjustment of side chains and torsion angles was performed. 81 solvent molecules, nine acetate ions and four glycerol molecules were subsequently added during refinement at chemically reasonable positions where $F_{\rm o} - F_{\rm c}$ difference densities exceeded 3σ.

In the last step of structure refinement, *phenix.refine* from the *PHENIX* program suite (Adams *et al.*, 2010) was applied to perform successive cycles of translation/libration/screw (TLS) refinement, resulting in an R factor of 21.6% and an $R_{\rm free}$ of 25.8% using all data in the range 30.0–2.7 Å. Residues 226–229 with weak electron density at the C-terminus were omitted.

The Ramachandran plot (Ramachandran *et al.*, 1963) indicates that 97.6% of the main-chain dihedral angles are located in the most favourable regions and 2.4% are found in additional allowed regions. Stereochemical and refinement parameters are summarized in Table 1. The coordinates of *Sa*TenA have been deposited in the Protein Data Bank with PDB code 4fn6.

2.4. Small-angle X-ray scattering

The radius of gyration $R_{\rm g}$ was evaluated using the Guinier approximation (Guinier, 1939) assuming that at very small angles ($s < 1.3/R_{\rm g}$) the intensity is represented as $I(s) = I(0)\exp[(sR_{\rm g})^2/-3]$. This parameter was also computed from the entire scattering data using the indirect transform package *GNOM* (Svergun, 1992), providing the pair distribution function of the particle $p(r)$ and also the maximum dimension $D_{\rm max}$. The excluded volume of the hydrated particle was computed from the small-angle portion of the data ($s <$ 0.25 Å^{-1}) using Porod's equation (Porod, 1982). Prior to this analysis an appropriate constant was subtracted from each data point to force the s^{-4} decay of the intensity at higher angles following Porod's law for homogeneous particles.

An *ab initio* model of TenA was generated using the program *DAMMIN* (Svergun, 1999). This program calculates the particle shape using an assembly of densely packed beads and employs simulated annealing to assign a compact interconnected model fitting the experimental data $I(s)$. *DAMMIN* runs were performed without symmetry and also imposing *P*222 symmetry of the particle. Ten *DAMMIN* runs were performed for each case and the obtained shapes superimposed well with each other. The models were further analyzed to determine their common structural features using the programs *DAMAVER* (Volkov & Svergun, 2003) and *SUPCOMB* (Kozin & Svergun, 2001). The latter program aligns two arbitrary low- or high-resolution models represented by ensembles of points by minimizing a dissimilarity measure called the normalized spatial discrepancy (NSD). The discrepancies are added and normalized against the average distances between the neighbouring points for the two models. Generally, NSD values close to unity indicate that the two

models are similar. Finally, the program *DAMAVER* (Volkov & Svergun, 2003) specifies the most typical model (*i.e.* that having the lowest average NSD with all of the other models in the set).

The scattering from the *Sa*TenA crystal structure was calculated with the program *CRYSOL* (Svergun *et al.*, 1995). Given the atomic coordinates, the program minimizes the discrepancy in the fit to the experimental intensity $I(s)$ by adjusting the excluded volume of the particle and the contrast of the hydration layer.

2.5. Site-directed mutagenesis of *Sa*TenA

In order to generate a monomeric *Sa*TenA mutant, two essential amino acids, Asp111 and Lys115, which stabilize the *Sa*TenA tetramer *via* hydrogen-bond interactions in the interface regions were identified and site-directed mutagenesis was carried out to change Asp111 to alanine as well as Lys115 to alanine. The *Sa*TenA mutant was expressed in *Escherichia coli* BLR (DE3) cells, purified *via* *Strep*-Tactin Sepharose according to Müller *et al.* (2009) and applied onto a Superdex 200 gel-filtration column (GE Healthcare, USA) for further characterization. Peak fractions were analyzed by SDS–PAGE. The presence of the D111A and K115A double mutation was verified by nucleotide sequencing (SeqLab, Germany).

2.6. Activity analysis

*Sa*TenA activity assays were carried out in a volume of 50 µl containing 100 m*M* Tris–HCl pH 7.5 and 0.05–20 m*M* thiamine (Sigma, USA). 75 µg of purified wild-type TenA or D111A-K115A mutant protein was added and incubated for 30 min at 310 K. The reaction was stopped by boiling the solutions for

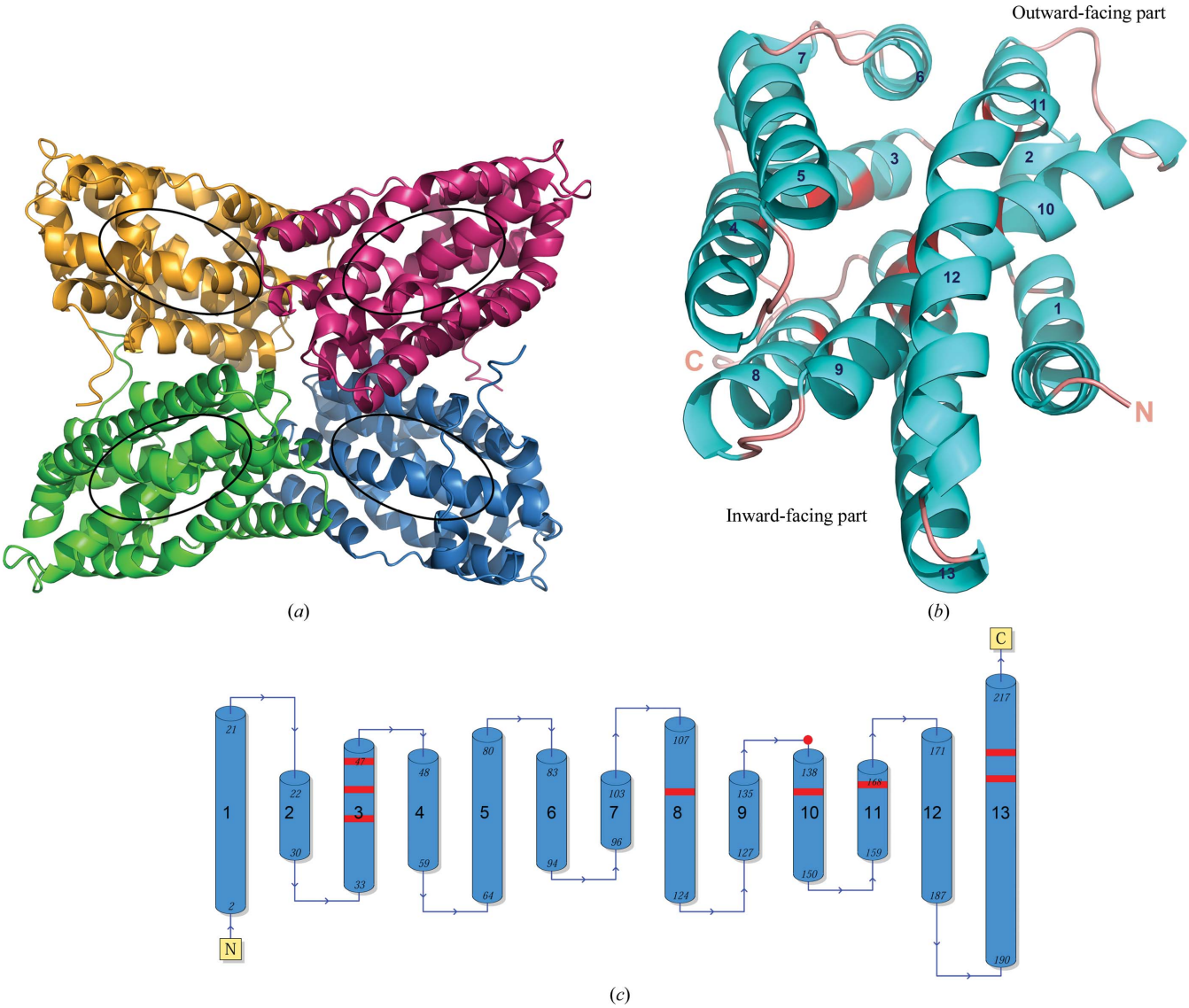

Figure 2
(*a*) Ribbon representation of the *Sa*TenA homotetramer. Monomers are indicated in four different colours. Ellipsoids indicate the active-site regions. (*b*) Cartoon plot of an *Sa*TenA monomer; active-site residue positions are indicated in red. Numbers in dark blue designate the α-helices, which are numbered from the N-terminus to the C-terminus. (*c*) Topology diagram of *Sa*TenA. The active-site residues are again indicated in red.

2 min and the reaction products were analyzed by an assay in which the amount of generated THZ-[^{33}P] was determined with the auxiliary enzyme *Sa*ThiM as described previously (Müller *et al.*, 2009). *De novo* synthesized THZ-[^{33}P] was quantified using an LS5000 CE scintillation detector (Beckman Coulter, USA). The kinetic parameters were calculated using the *GraphPad Prism* 5 software (GraphPad Software, USA) according to Wrenger *et al.* (2006) and are summarized in Table 2.

2.7. Protease stability tests

To analyze the structural stability of the *Sa*TenA wild-type tetramer *versus* the *Sa*TenA monomeric mutant in the presence of proteases, 200 µg of wild-type and mutant TenA were comparatively hydrolyzed by applying subtilisin from *B. licheniformis* in one experiment and trypsin from bovine pancreas in a second experiment (both using the Floppy Choppy Kit, Jena BioScience, Germany) both in a 1:1000 ratio. The hydrolytic effect of the selected proteases was monitored for 52 h. 5 µg samples were taken at different time intervals, incubated with SDS sample buffer and applied to SDS–PAGE analysis.

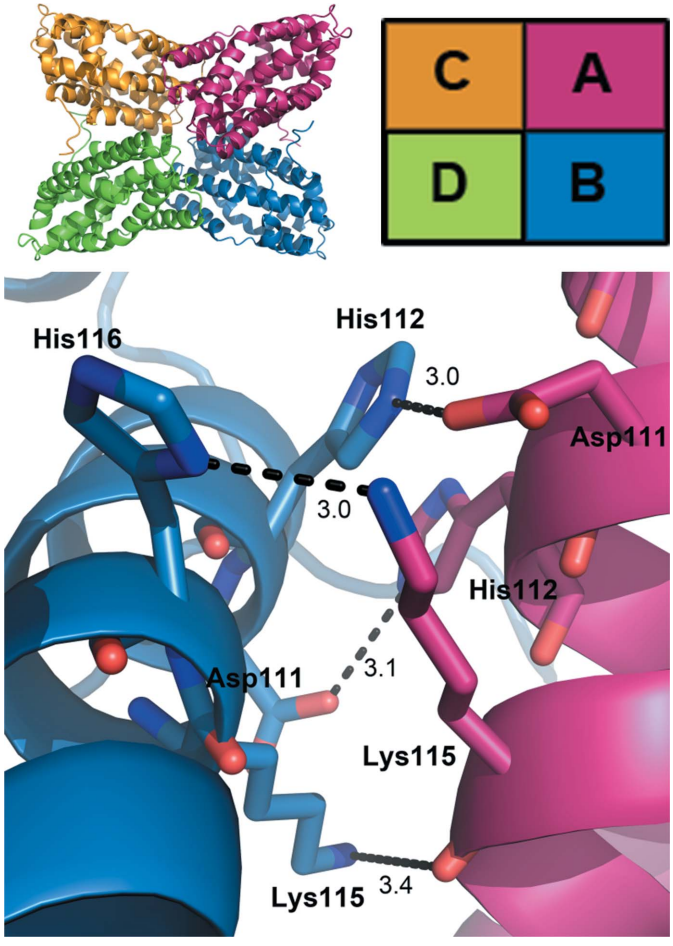

Figure 3
The cartoon plot on the upper left shows the four monomers in different colours. The schematic drawing on the upper right indicates the four amino-acid chains using the same colour code. An enlargement of the Asp111 and Lys115 mutation site within the *A*–*B* interface region shows the interaction partners. The corresponding hydrogen bonds are shown as dashed lines and numbers indicate the hydrogen-bond lengths in Å.

Table 2
Kinetic parameters of WT *Sa*TenA and the monomeric D111A-K115A *Sa*TenA mutant.

	K_m (m*M*)	Specific activity (mU mg^{-1})	k_{cat} (ms^{-1})	k_{cat}/K_m (M^{-1} s^{-1})
WT *Sa*TenA	1.40 ± 0.19	9.12 ± 0.16	4.07 ± 0.07	2.92 ± 0.05
D111A-K115A mutant	2.25 ± 0.17	15.31 ± 0.24	6.80 ± 0.11	3.04 ± 0.05

Table 3
Structural details of the *Sa*TenA homotetramer interface regions and hydrogen-bond as well as hydrophobic interactions.

A–*B* ≃ *C*–*D* and *A*–*C* ≃ *B*–*D*. For every interface, the buried surface and the number of residues involved is shown. The homotetramer is stabilized by intermolecular contacts through hydrogen bonds and hydrophobic interactions.

Chains	No. of interface residues	Interface area (Å^2)	No. of hydrogen bonds	No. of hydrophobic interactions
A–*B*	21:21	1072:1075	3	105
C–*D*	21:22	1091:1075	6	112
A–*C*	12:13	782:748	1	29
B–*D*	12:11	765:759	1	35
A–*D*	3:3	136:136	4	25
B–*C*	3:3	129:135	4	26

3. Results and discussion

3.1. Crystal structure

The refined X-ray structure of *Sa*TenA is a rectangular-shaped homotetramer with dimensions of 84 × 54 × 50 Å, as shown in Fig. 2(*a*). Each monomer has dimensions of approximately 33 × 48 × 26 Å (Fig. 2*b*). In the crystal structure, only residues 226–229 in the C-terminal region were disordered and were not included in the model. In the tetrameric assembly of *Sa*TenA, the active-site regions of all monomers within the homotetramer are similarly oriented, as indicated in Fig. 2(*a*). The secondary structure of *Sa*TenA is predominately α-helical, with short loops connecting the 13 overall α-helices (Fig. 2*c*). A relatively deep and negatively charged pocket forms the substrate-binding region (described in the following section). The overall structure is homologous to other reported TenA counterparts, *e.g. S. epidermidis* TenA (PDB entry 3no6; Joint Center for Structural Genomics, unpublished work), *Pyrococcus horikoshii* TenA and *B. subtilis* TenA (Barison *et al.*, 2009; Toms *et al.*, 2005). Each monomer in the quaternary structure interacts with the three other monomers and the homotetramer is well stabilized by distinct intermolecular hydrophobic contacts and hydrogen bonds. The interface regions were evaluated using the *PDBsum* server (Laskowski *et al.*, 1997) and data describing the interface are summarized in Table 3. A total of 36 residues of each monomer are involved and located in interface regions of the homotetramer. The mean value of the area buried involving 21 amino acids of each monomer in the *A*–*B* or the equivalent *C*–*D* interface is 1078 Å^2, and corresponds to 9.4% of the total

surface of a monomer. The interface is well stabilized by an almost antiparallel hydrogen-bond pattern of residues located on helices H8 in the respective monomers, as shown in Fig. 3. In contrast, only three residues are involved in the *A*–*D* and the corresponding *B*–*C* interface; however, this interface is stabilized by two antiparallelly arranged hydrogen bonds formed by Arg124 and Glu125 of each monomer, both located in the loop connecting helices H8 and H9. In total, besides hydrophobic interactions 18 intermolecular hydrogen bonds stabilize the homotetramer. The buried surface for all monomers is 7794 Å^2, which corresponds to 20% of the total surface area of 38 046 Å^2 of the homotetramer.

3.2. The active site

The orientation and location of the active-site residues is well conserved in all TenA enzymes. The active-site architecture of *B. subtilis* TenA (Toms *et al.*, 2005) with bound HMP has been well characterized previously and was used to identify the active site of *Sa*TenA by superimposition onto the native *Sa*TenA structure. Our model shows a highly similar spatial architecture of the active site and suggests similar substrate binding (Fig. 4*a*) in *Sa*TenA. Additionally, a relatively deep acidic active-site pocket, as described for other TenA orthologues, was apparent (Fig. 4*b*). Based on the model, the active site is formed by helices H3, H8, H10, H11 and H13 and is located almost in the centre of each monomer. As a result, the *Sa*TenA homotetramer comprises four active sites with the proposed catalytic residues Asp44, Cys137 and Glu208. The residues Tyr47, Tyr113, Tyr167 and Phe211 in the active site could support the π-stacking (Toms *et al.*, 2005) geometry of the ligand, as shown in Fig. 4(*a*). Bacterial thiaminases bind a substrate by a hydrogen bond between the carboxylate side chain of a glutamic acid and the N1 atom of the pyrimidine ring. In *Sa*TenA this residue is very likely to be Glu208. Further, the carboxylate side chain of Asp44 is positioned to stabilize and orient the binding of the substrate, which is additionally coordinated by a hydrogen bond between the hydroxyl group of Tyr163 and N4 of the pyrimidine ring in *B. subtilis* TenA. The respective residues Asp44

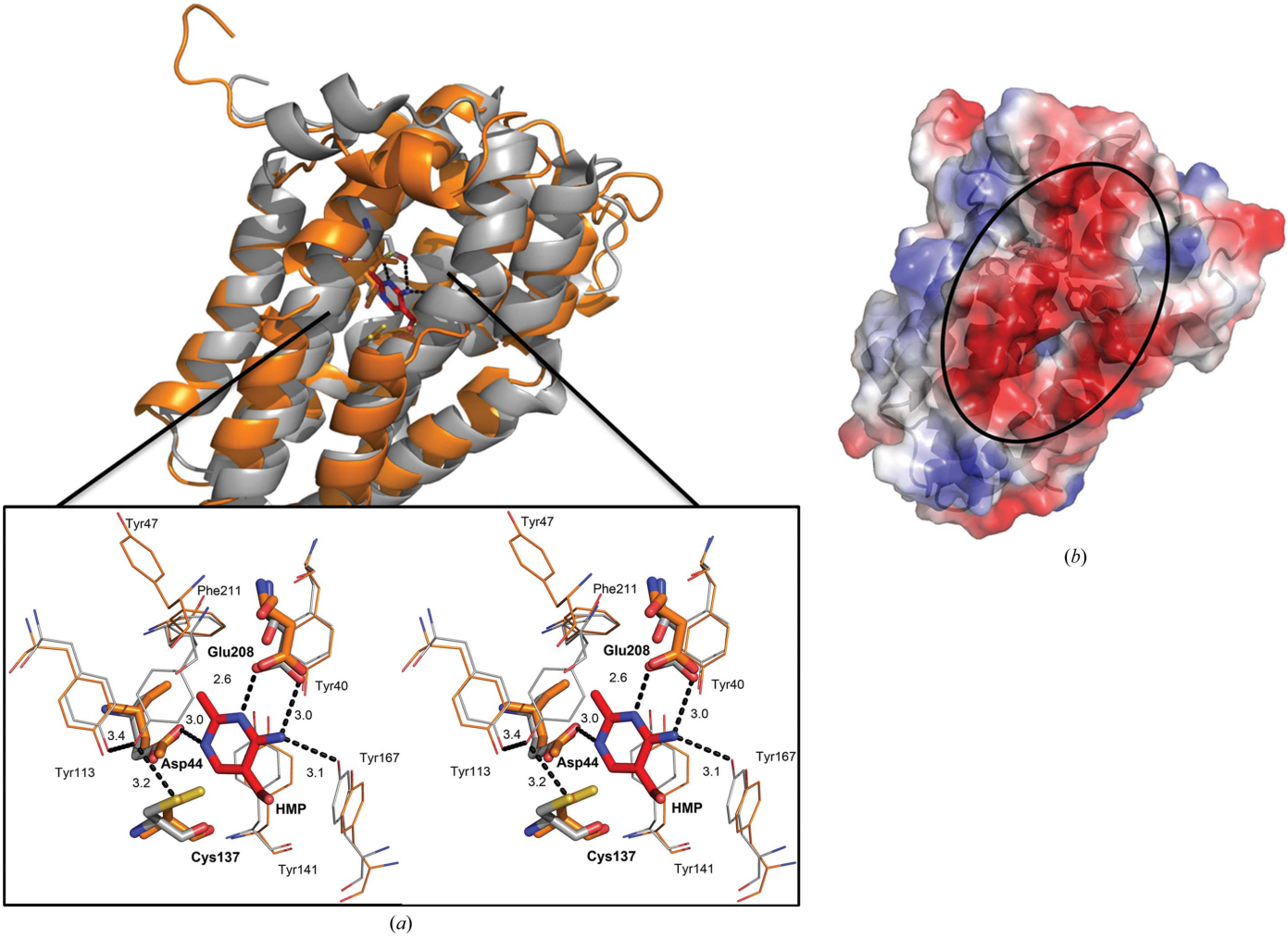

Figure 4
(*a*) Superimposition of *Sa*TenA (shown in orange) and *Bs*TenA (shown in grey), the latter cocrystallized with HMP (PDB entry 1yak; Toms *et al.*, 2005). A stereo enlargement of the active-site residues is shown in stick representation. The ligand HMP is displayed in red. Hydrogen-bond interactions are shown as dotted lines. (*b*) Electrostatic surface representation of *Sa*TenA with positive charge in blue and negative charge in red. Active-site residues are highlighted as sticks. The ellipsoid marks the negatively charged (red) binding pocket.

Table 4
SAXS data-collection and derived parameters for *Sa*TenA.

Data-collection parameters	
Instrument	EMBL beamline X33
Wavelength (Å)	1.5
s range (Å^{-1})	0.01–0.6
Exposure time (s)	120
Concentration range (mg ml^{-1})	1.2–7.2
Temperature (K)	278
Structural parameters	
R_g (Å) (from Guinier)	33 ± 2
D_{max} (Å)	110 ± 10
Molecular weight from the hydrated volume (kDa)	105 ± 20
Monomeric molecular weight calculated from the sequence (kDa)	26.8

and Tyr167 match these positions in *Sa*TenA. In our superimposition model, the side chain of the catalytic residue Cys137 is positioned close to the C2 atom of the pyridine ring and would be required for the cleavage of thiamine into its respective heterocycles, as seen for Cys135 in *B. subtilis* TenA.

3.3. Quaternary structure in solution

To analyze and validate the oligomeric conformation of *Sa*TenA in solution, SAXS data were collected (Fig. 5*a*, blue circles; Table 4). Given the uncertainty in determining the protein concentration, it was difficult to estimate the molecular weight of the solute from the forward scattering. This value could, however, be assessed from the Porod volume of the particle in solution, which is equal to (168 ± 17) × 10^3 Å^3. Noting that the average ratio between the molecular weight in daltons and the hydrated volume in Å^3 is 0.625 (Petoukhov & Svergun, 2012), a molecular-weight estimate of 105 ± 21 was obtained, which corresponds to a *Sa*TenA tetramer.

The experimental radius of gyration R_g and the maximum particle size D_{max} (33 ± 2 and 110 ± 10 Å, respectively) point to an extended structure. The low-angle data (up to s = 0.18 Å^{-1}) can be fitted (χ = 1.4) with a 69 × 69 × 38 Å rectangular prism using the program *BODIES* (Konarev *et al.*, 2003; fit not shown). The low-resolution shape of *Sa*TenA was reconstructed *ab initio* using the bead modelling program *DAMMIN* (Svergun, 1999), employing the range of scattering vectors up to s = 0.25 Å^{-1} and imposing *P*222 symmetry. The most probable model out of ten reconstructions shown in Fig. 5(*b*) fits the experimental data with χ = 1.0 (Fig. 5*a*, red

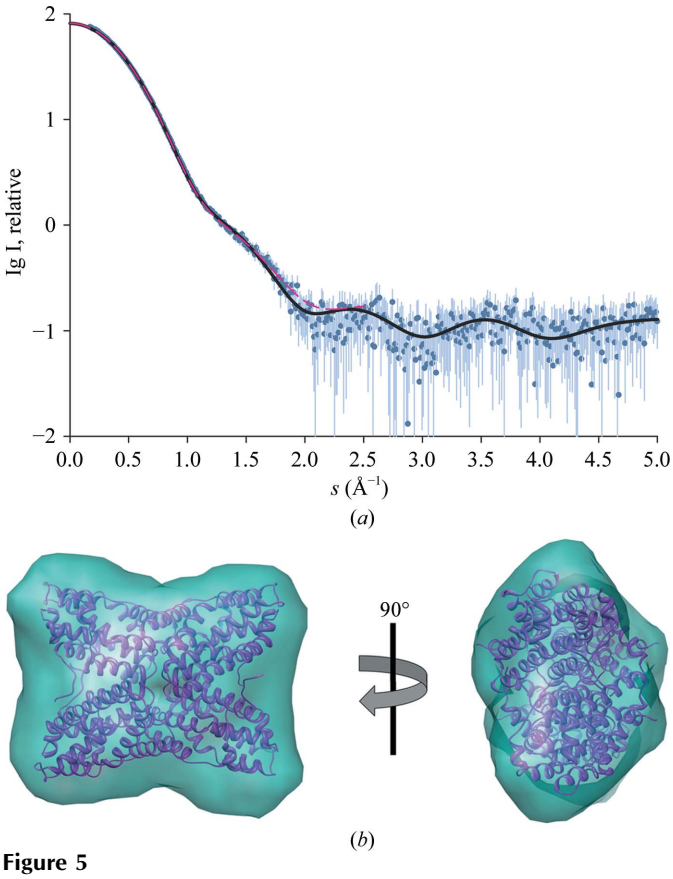

Figure 5
(*a*) Processed solution-scattering data of TenA. Experimental data are displayed as blue circles. The *CRYSOL* (Svergun *et al.*, 1995) fit based on the crystal structure is shown as a black line and the *ab initio* model fit is shown as a red dashed line. (*b*) Front and side view of tetrameric TenA. The *ab initio* shape is shown in turquoise and is superimposed with the crystal structure shown in ribbon representation.

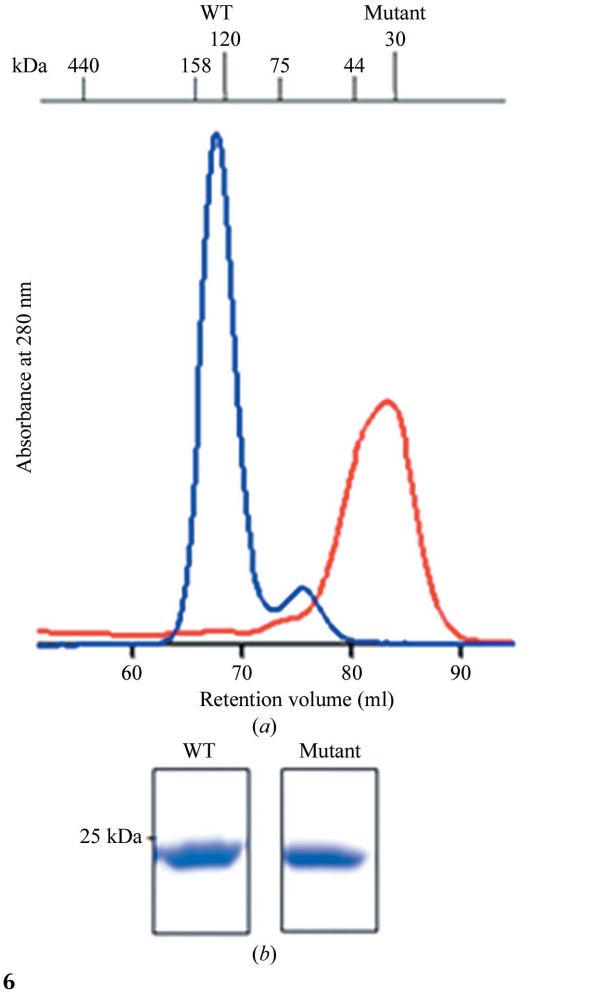

Figure 6
Gel-filtration profile comparison for WT *Sa*TenA (blue) and the D111A-K115A mutant (red). (*a*) The absorbance at 280 nm was plotted against the respective retention volume to determine the molecular weight of the peak fractions (the molecular-weight marker is shown above). (*b*) The peak fractions of the gel-filtration analysis were applied onto an SDS gel, showing pure *Sa*TenA bands with the expected molecular weight for both the WT and the mutant.

dashed line). This model is in good agreement with the crystal structure. Finally, the crystal structure yields a good fit (χ = 1.1; Fig. 5*a*, black line) to the experimental data. All of these results unequivocally indicate that the crystallographic tetramer of *Sa*TenA is the biologically active assembly observed in solution.

3.4. Structural comparison

A *BLAST* search revealed that *Sa*TenA shares 58% amino-acid sequence identity with *S. epidermidis* TenA (PDB entry 3no6), 24% identity with *Helicobacter pylori* TenA (PDB entry 2rd3; Barison *et al.*, 2009), 24% identity with *P. horikoshii* TenA (PDB entry 1udd; Itou *et al.*, 2004) and 23% identity with *B. subtilis* TenA (PDB entry 1yaf; Toms *et al.*, 2005), with corresponding C^{α} r.m.s.d. values of 0.7, 1.6, 1.6 and 1.5 Å and maximum displacements of 3.8, 6.3, 5.0 and 6.1 Å for the structures 3no6, 2rd3, 1udd and 1yaf, respectively, as calculated with *LSQKAB* (Kabsch, 1976). For r.m.s.d. calculations amino acids corresponding to a mainly distorted helical region at the surface of the TenA proteins were omitted. The overall fold is conserved for all TenA proteins, with a deep acidic ligand-binding pocket showing a high structural homology and a conserved active site.

3.5. Mutagenic studies

To identify the amino acids in the interface regions of the monomers which are essential in stabilizing the tetrameric conformation, the *PDBsum* server was applied to provide information for all noncovalent interactions (Laskowski *et al.*, 1997). The results are summarized in Table 3. After further detailed manual inspection of all interactions in the interface regions, the amino acids Asp111 and Lys115 located within the interfaces *A*–*B* and *C*–*D* (Fig. 3) were identified to be most important in stabilizing the homotetramer by forming the intermolecular hydrogen bonds Asp111–His112 and Lys115–His116. Consequently, site-directed mutagenesis was applied and comparative gel-filtration analysis (Fig. 6) of wild-type and D111A-K115A *Sa*TenA clearly confirmed monomer formation of the *Sa*TenA mutant.

3.6. Enzymatic activity assays

Wild-type (WT) and mutated *Sa*TenA were used to perform comparative activity assays. While the mutant revealed an

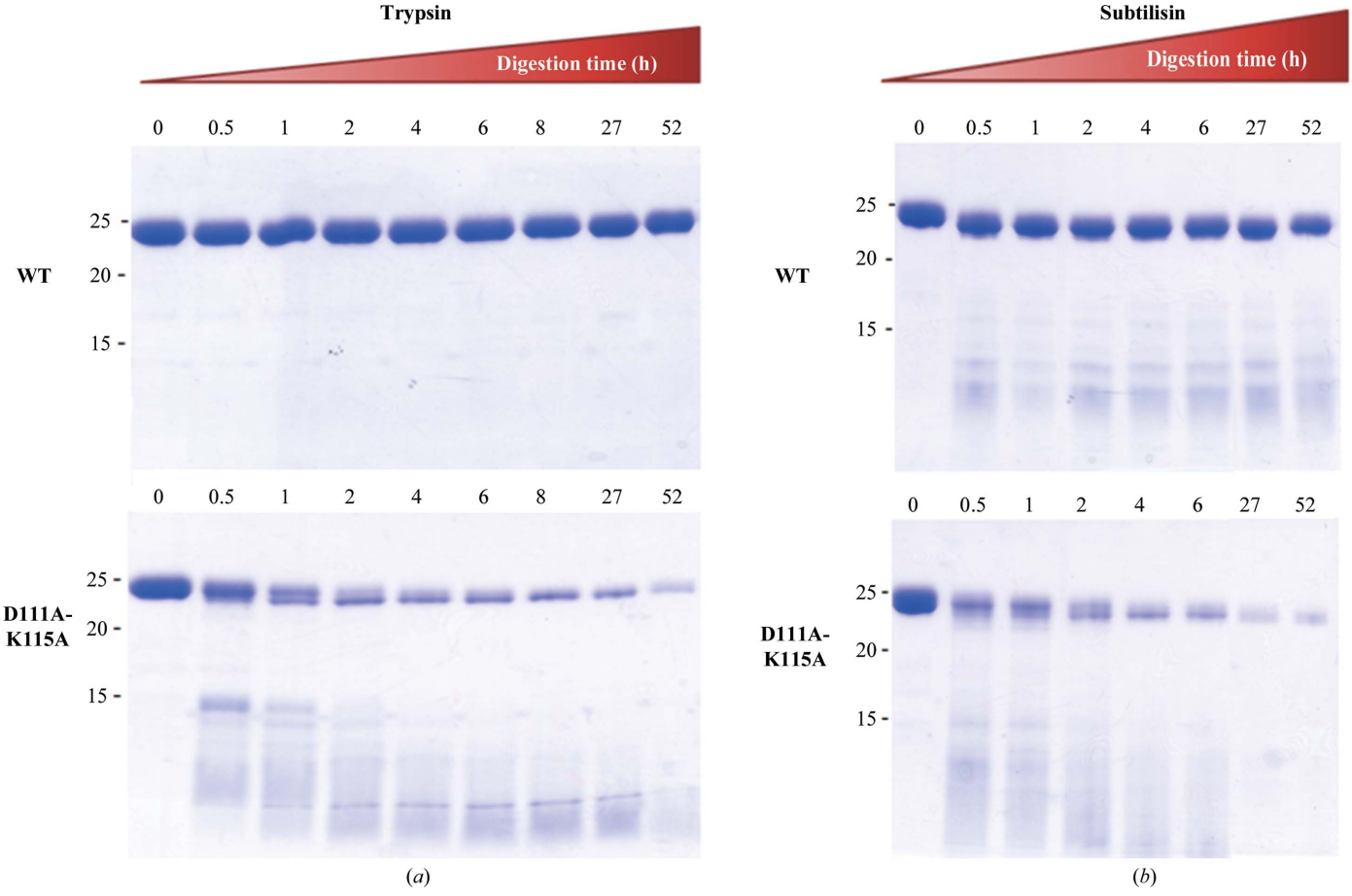

Figure 7
SDS gels showing the hydrolytic effect of trypsin (*a*) and subtilisin (*b*) towards WT *Sa*TenA (upper gels) and the D111A-K115A *Sa*TenA mutant (lower gels). The hydrolytic effects were monitored up to 52 h in time intervals as indicated at the top of the gels. The proteases were added to the *Sa*TenA protein samples in a 1:1000 ratio and incubated at room temperature. The numbers on the left side of the gels show the marker band sizes (in kDa) and the numbers at the top of the gels indicate incubation times. The SDS gel was stained with Coomassie dye.

approximately doubled K_m value in comparison to the WT, the specific activity is in the same range for both (WT, 9.12 ± 0.16 U mg^{-1}; mutant, 15.31 ± 0.24 U mg^{-1}) as is the turnover number (k_{cat}; WT, 4.07 ± 0.07 ms^{-1}; mutant, 6.8 ± 0.11 ms^{-1}) and the efficiency k_{cat}/K_m (WT, 2.92 ± 0.05; mutant, 3.04 ± 0.05). The active site is not located in the interface regions; therefore, it was expected that the enzyme activity of the monomeric D111A-K115A *Sa*TenA mutant is not significantly altered in comparison to the WT (Table 2).

3.7. Effect of trypsin and subtilisin on mutant and WT *Sa*TenA

During exponential growth of bacteria in *S. aureus* infections, exotoxin proteases are expressed and secreted into the host tissue to acquire nutrients. In contrast to cysteine proteases, against which endogenous inhibitors offer protection, no such protection is evident to prevent the degradation of cytoplasmic proteins by serine proteases during their passage through the cytosol in *S. aureus* (Rzychon *et al.*, 2003). Only the signal sequence directs the protease to the extracellular compartment and assures its inactive state (Popowicz *et al.*, 2006).

We performed comparative stability assays with the *Sa*TenA homotetrameric WT and monomeric mutant to test whether there were differences in proteinase resistance. The results clearly confirmed that WT *Sa*TenA is not affected by trypsin and remained stable during the entire exposure to trypsin during the hydrolytic experiment. After 52 h no degradation bands were observed for the WT protein. In contrast, the mutant protein was already partially digested after 30 min and was almost totally hydrolyzed after 52 h, as shown in Fig. 7(*a*). The same experiment was carried out using subtilisin. In contrast to the experiment applying trypsin, the WT protein was slightly digested. However, mutated *Sa*TenA was hydrolyzed more substantially and was almost completely hydrolyzed after 52 h (Fig. 7*b*). The results confirm the assumption that bacterial thiaminases, which are all reported to be functional as tetramers (Itou *et al.*, 2004; Toms *et al.*, 2005), need to have the structural rigidity and stability provided by oligomer formation to remain enzymatically active in an environment of highly active proteinases. The bifunctional enzyme THI20 from yeast also has a dimeric TenA domain, which is flanked by the ThiD domain (French *et al.*, 2011), supporting the assumption that high-molecular assemblies are more stable and protective against proteases. Finally, these results support the hypothesis that the enhanced structural stability of oligomers also provides the required protection against serine proteases passing through the *S. aureus* cytosol and serine protease domains which are part of the degradome of *S. aureus* (Maurizi *et al.*, 1990; Bochtler *et al.*, 1997).

4. Conclusion

In order to obtain structural and functional data on *Sa*TenA, we used crystallography and SAXS measurements in combination with enzymatic assays and protein-stability investigations. These analyses revealed for the first time that the enzymatic activity is not dependent on the oligomeric state of *Sa*TenA. During proliferation, *S. aureus* secretes proteases to acquire nutrients from host tissue. However, the tetrameric conformation of *Sa*TenA provides enhanced stability and protection against such proteolytic enzymes compared with the monomeric *Sa*TenA mutant.

This project was funded by the Hamburg Ministry of Science and Research and Joachim Herz Stiftung as part of the Hamburg Initiative for Excellence in Research (LEXI), Hamburg School for 'Structure and Dynamics in Infection (SDI)', as well as by grants from the Deutscher Akademischer Austauschdienst (DAAD) and the Deutsche Forschungsgemeinschaft (DFG, WR124/2). CW is a 'Jovem Pesquisador' of the Fundação de Amparo à Pesquisa do Estado de São Paulo (FAPESP, 2009/54325-2).

References

Adams, P. D. *et al.* (2010). *Acta Cryst.* D**66**, 213–221.
Barison, N., Cendron, L., Trento, A., Angelini, A. & Zanotti, G. (2009). *FEBS J.* **276**, 6227–6235.
Begum, A., Drebes, J., Perbandt, M., Wrenger, C. & Betzel, C. (2011). *Acta Cryst.* F**67**, 51–53.
Blanchet, C. E., Zozulya, A. V., Kikhney, A. G., Franke, D., Konarev, P. V., Shang, W., Klaering, R., Robrahn, B., Hermes, C., Cipriani, F., Svergun, D. I. & Roessle, M. (2012). *J. Appl. Cryst.* **45**, 489–495.
Bochtler, M., Ditzel, L., Groll, M. & Huber, R. (1997). *Proc. Natl Acad. Sci. USA*, **94**, 6070–6074.
Dinges, M. M., Orwin, P. M. & Schlievert, P. M. (2000). *Clin. Microbiol. Rev.* **13**, 16–34.
Du, Q., Wang, H. & Xie, J. (2011). *Int. J. Biol. Sci.* **7**, 41–52.
Emsley, P. & Cowtan, K. (2004). *Acta Cryst.* D**60**, 2126–2132.
Fey, P. D., Saïd-Salim, B., Rupp, M. E., Hinrichs, S. H., Boxrud, D. J., Davis, C. C., Kreiswirth, B. N. & Schlievert, P. M. (2003). *Antimicrob. Agents Chemother.* **47**, 196–203.
Franke, D., Kikhney, A. G. & Svergun, D. I. (2012). *Nucl. Instrum. Methods Phys. Res. A*, **689**, 52–59.
French, J. B., Begley, T. P. & Ealick, S. E. (2011). *Acta Cryst.* D**67**, 784–791.
Guinier, A. (1939). *Ann. Phys.* **12**, 161–237.
Itou, H., Yao, M., Watanabe, N. & Tanaka, I. (2004). *Acta Cryst.* D**60**, 1094–1100.
Jenkins, A. H., Schyns, G., Potot, S., Sun, G. & Begley, T. P. (2007). *Nature Chem. Biol.* **3**, 492–497.
Kabsch, W. (1976). *Acta Cryst.* A**32**, 922–923.
Kauffman, C. A., Terpenning, M. S., He, X., Zarins, L. T., Ramsey, M. A., Jorgensen, K. A., Sottile, W. S. & Bradley, S. F. (1993). *Am. J. Med.* **94**, 371–378.
Konarev, P. V., Volkov, V. V., Sokolova, A. V., Koch, M. H. J. & Svergun, D. I. (2003). *J. Appl. Cryst.* **36**, 1277–1282.
Kozin, M. B. & Svergun, D. I. (2001). *J. Appl. Cryst.* **34**, 33–41.
Laskowski, R. A., Hutchinson, E. G., Michie, A. D., Wallace, A. C., Jones, M. L. & Thornton, J. M. (1997). *Trends Biochem. Sci.* **22**, 488–490.
Lewis, K. (2012). *Nature (London)*, **485**, 439–440.
Lowy, F. D. (1998). *N. Engl. J. Med.* **339**, 520–532.
Maurizi, M. R., Clark, W. P., Katayama, Y., Rudikoff, S., Pumphrey, J., Bowers, B. & Gottesman, S. (1990). *J. Biol. Chem.* **265**, 12536–12545.
Müller, I. B., Bergmann, B., Groves, M. R., Couto, I., Amaral, L., Begley, T. P., Walter, R. D. & Wrenger, C. (2009). *PLoS One*, **4**, e7656.
Murshudov, G. N., Skubák, P., Lebedev, A. A., Pannu, N. S., Steiner, R. A., Nicholls, R. A., Winn, M. D., Long, F. & Vagin, A. A. (2011). *Acta Cryst.* D**67**, 355–367.

Pang, A. S.-H., Nathoo, S. & Wong, S.-L. (1991). *J. Bacteriol.* **173**, 46–54.
Petoukhov, M. V. & Svergun, D. I. (2012). *Int. J. Biochem. Cell Biol.* **45**, 429–437.
Pohl, M., Sprenger, G. A. & Müller, M. (2004). *Curr. Opin. Biotechnol.* **15**, 335–342.
Popowicz, G. M., Dubin, G., Stec-Niemczyk, J., Czarny, A., Dubin, A., Potempa, J. & Holak, T. A. (2006). *J. Mol. Biol.* **358**, 270–279.
Porod, G. (1982). *Small-Angle X-ray Scattering*, edited by O. Glatter & O. Kratky, pp. 17–51. London: Academic Press.
Powers, T. & Bingham, D. (1990). *Am. J. Health Syst. Pharm.* **47**, 1781–1784.
Ramachandran, G. N., Ramakrishnan, C. & Sasisekharan, V. (1963). *J. Mol. Biol.* **7**, 95–99.
Rzychon, M., Sabat, A., Kosowska, K., Potempa, J. & Dubin, A. (2003). *Mol. Microbiol.* **49**, 1051–1066.
Spellberg, B., Bartlett, J. G. & Gilbert, D. N. (2013). *N. Engl. J. Med.* **368**, 299–302.
Svergun, D. I. (1992). *J. Appl. Cryst.* **25**, 495–503.
Svergun, D. I. (1999). *Biophys. J.* **76**, 2879–2886.
Svergun, D., Barberato, C. & Koch, M. H. J. (1995). *J. Appl. Cryst.* **28**, 768–773.
Toms, A. V., Haas, A. L., Park, J.-H., Begley, T. P. & Ealick, S. E. (2005). *Biochemistry*, **44**, 2319–2329.
Tumbarello, M., Tacconelli, E., de Gaetano, K., Ardito, F., Pirronti, T., Cauda, R. & Ortona, L. (1998). *J. Acquir. Immune Defic. Syndr.* **18**, 39–45.
Vagin, A. & Teplyakov, A. (2010). *Acta Cryst.* D**66**, 22–25.
Volkov, V. V. & Svergun, D. I. (2003). *J. Appl. Cryst.* **36**, 860–864.
Weinke, T., Schiller, R., Fehrenbach, F. J. & Pohle, H. D. (1992). *Eur. J. Clin. Microbiol. Infect. Dis.* **11**, 985–989.
Winn, M. D. *et al.* (2011). *Acta Cryst.* D**67**, 235–242.
Wrenger, C., Eschbach, M. L., Müller, I. B., Laun, N. P., Begley, T. P. & Walter, R. D. (2006). *Biol. Chem.* **387**, 41–51.